Absolute measurements of x-ray backlighter sources at energies above 10 keV[a)]

B. R. Maddox,[1,b)] H. S. Park,[1] B. A. Remington,[1] C. Chen,[1] S. Chen,[1] S. T. Prisbrey,[1] A. Comley,[2] C. A. Back,[3] C. Szabo,[4] J. F. Seely,[4] U. Feldman,[5] L. T. Hudson,[6] S. Seltzer,[6] M. J. Haugh,[7] and Z. Ali[7]
[1]*Lawrence Livermore National Laboratory, Livermore, California 94550, USA*
[2]*Atomic Weapons Establishment, Aldermasten, Reading RG7 4PR, United Kingdom*
[3]*General Atomics, San Diego, California 92121, USA*
[4]*Naval Research Laboratory, Washington D.C. 20375, USA*
[5]*ARTEP Inc., Ellicott City, Maryland 21042, USA*
[6]*National Institute of Standards and Technology, Gaithersburg, Maryland 20899, USA*
[7]*NSTEC, Livermore, California 94550, USA*

(Received 1 December 2010; accepted 28 February 2011; published online 19 May 2011)

Line emission and broadband x-ray sources with x-ray energies above 10 keV have been investigated using a range of calibrated x-ray detectors for use as x-ray backlighters in high energy density (HED) experiments. The conversion efficiency of short- and long-pulse driven Mo and Ag line-emission backlighters at 17 and 22 keV was measured to investigate the crossover region between short- and long-pulse conversion efficiency. It was found that significant 17 and 22 keV line emissions were observed using a 3 ω, 1 ns long-pulse drive for Mo and Ag targets and a comparison between the measured Mo x-ray spectrum and calculations using an atomic physics code suggests that the line emission is due to thermal emission from N-like Mo atoms. Electron temperatures derived from fits to the continuum region of the x-ray spectra agree well with the T_{hot} scaling as $100 \times (I\lambda^2)^{1/3}$. The continuum emissions from empty and 1 atm Kr-filled imploded CH shell targets were also measured for the use as broadband backlighters. © *2011 American Institute of Physics*. [doi:10.1063/1.3582134]

I. INTRODUCTION

There are many high energy density (HED) experiments that require efficient, line-emission, or broadband x-ray sources with photon energies greater than 10 keV. Examples of such experiments are shown in Fig. 1. High energy radiography to measure the growth of Rayleigh–Taylor unstable features for tests of strength models of Ta requires a line-emission backlighter at 22 keV to penetrate the $\sim$50 μm thick Ta targets. Time-resolved Bragg diffraction of Mo to probe the lattice dynamics of shocked BCC metals requires a 17 keV backlighter to probe a sufficient number of lattice planes. White-light, or broadband transmission Laue diffraction of Ta or Mo to study the ultra-high pressure phase and twinning in BCC metals requires a bright broadband source between 10 and 25 keV.

Traditionally, laser-generation line sources with photon energies below about 10 keV have been created by irradiating a thin foil using a 3 ω long-pulse laser of around 1 ns pulse length and 10^{15} W/cm^2 as shown in Fig. 2(a).[1] Line emission from these sources is the result of thermal emission of highly ionized atoms in the coronal region of the plasma, near the ablation front. The dominant line emission that has been studied is the He-α line that is the result of 2p$\rightarrow$1s transitions from He-like ions. For x-ray line energies above 10 keV, the invention of petawatt lasers has allowed the creation of essentially cold Kα sources. A high intensity, short-pulse laser with a pulse length of $<$100 ps and intensity $>10^{17}$ W/cm ^{2} is used to drive supra-thermal electrons into a cold, dense foil.[2] This is shown schematically in Fig. 2(b). The effective temperature of the supra-thermal or "hot" electron distribution has been shown to scale as $\sim(I\lambda^2)^{1/3}$ (Ref. 3). These hot electrons collide with atoms in the foil, knocking out core electrons. Inner shell transitions between these core states produce characteristic line radiation, the most commonly used being Kα and Kβ.

Many efforts have been made to characterize the conversion efficiency (CE) of laser energy into line emission photons of long-pulse thermal and short-pulse Ka backlighters. Figure 3 gives summaries of work performed by Back *et al.*[1] and Workman *et al.*[4] on long-pulse He-α backlighters, and Park *et al.*[5] on short-pulse backlighters. At low energy, thermal backlighters are very efficient, converting up to 1% of the laser energy into He-α photons. The dashed lines in Fig. 3 are fits to the experimental data and show that at higher x-ray energies thermal backlighters rapidly drop in efficiency. At 40 keV line energies, short-pulse Kα backlighters should be $\sim$2 orders of magnitude more efficient. The two slopes overlap at 17 keV, suggesting that it is possible to drive 17 keV thermal line emission using a long-pulse laser drive with comparable efficiency to a short-pulse driver. This would have many advantages over a petawatt backlighter, such as significantly lower high-energy bremsstrahlung background emission, and would allow 17 keV line-emission backlighters on facilities that do not currently have petawatt capability. However, no data existed in this crossover region between thermal and Kα conversion efficiency prior to this study.

[a)]Paper QI3 3, Bull. Am. Phys. Soc. **55**, 286 (2010).
[b)]Invited speaker.

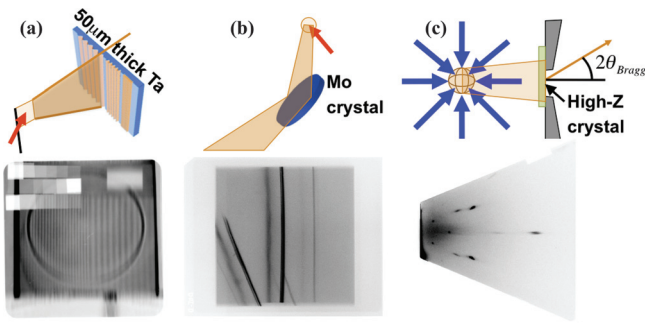

FIG. 1. (Color online) Example experiments utilizing >10 keV line emission or broadband x-ray sources. (a) High energy radiography to measure the growth of Rayleigh–Taylor unstable features as a sensitive test of strength models of Ta requires a line-emission backlighter at 22 keV to penetrate the ~50 μm thick Ta targets. (b) Time-resolved Bragg diffraction of Mo to probe the lattice dynamics of shocked BCC metals requires a 17 keV backlighter to probe a sufficient number of lattice planes. (c) White-light or broadband transmission Laue diffraction of Ta or Mo to study the ultra-high pressure phase and twinning in BCC metals requires a bright broadband source between 10 and 25 keV.

Broadband sources of x-rays can be produced in a variety of ways including dynamic hohlraums, gas bag targets, and underdense foam targets. This paper will focus on imploded CH shell backlighters, as the source size is small (~100 μm) and the x-ray emission time is short (~100 ps). Figure 4 shows a diagram of the imploded CH shell scheme. A number of symmetric lasers are used to implode a spherical shell capsule with a diameter on the order of 1 mm, and a wall thickness on the order of 10 μm. The inside of the shell is typically filled with a low-Z gas, such as H_2, that is compressed as the shell implodes. As the gas reaches a peak compression, the shell stagnates at the center producing a bright burst of bremsstrahlung radiation. Measurements of the absolute x-ray yield of these types of targets are scarce. Yaakobi *et al*. measured the absolute x-ray yield from 4.5 to 7 keV for a H_2-D_2 filled implosion capsule; however, no measurements exist for broadband emission of these targets above 10 keV.

This paper will present absolute measurements of x-ray spectra from long- and short-pulse line-emission backlighters at 17 and 22 keV as well as from an imploded CH shell broadband backlighter. The first section will introduce the experimental setup and the various x-ray diagnostics used to measure x-rays from 10 keV to over 1 MeV. An integrated measurement using these diagnostics will be presented for a short-pulse driven 22 keV Ag line-emission backlighter. The spectra from long- and short-pulse driven Mo and Ag line-emission backlighters will then be presented. Finally, the x-ray spectra from unfilled and Kr-filled imploded CH shell backlighters between 10 and 25 keV will be presented and compared with measurements by Yaakobi *et al*. at lower x-ray energies.

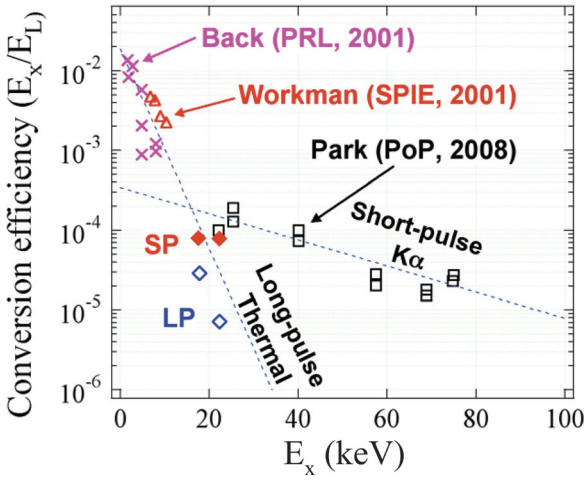

FIG. 3. (Color online) A compilation of conversion efficiency (CE) of laser energy, E_x, into line emission of x-ray energy E_x for long- and short-pulse driven backlighter targets. Also shown is the conversion efficiency of long- and short-pulse driven Mo and Ag backlighters at 17 and 22 keV measured in this study using single photon counting.

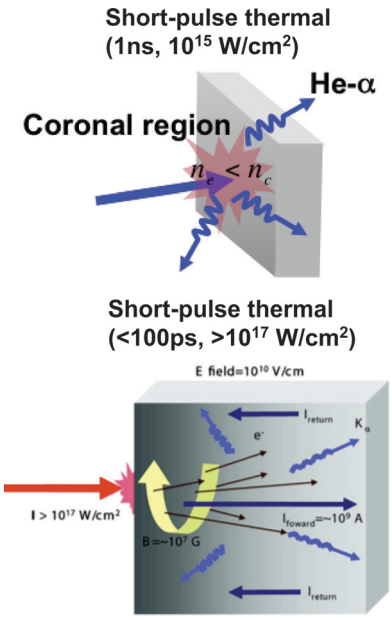

FIG. 2. (Color online) X-ray generation mechanisms for use as diagnostic backlighter sources (a) Thermal He-α x-ray emission is generated in the hot coronal region of a long-pulse produced plasma. (b) Supra-thermal, "hot" electrons are produced when a short-pulse, high intensity laser interacts with a solid foil target. These hot electrons generate Kα photons when they collide with atoms.

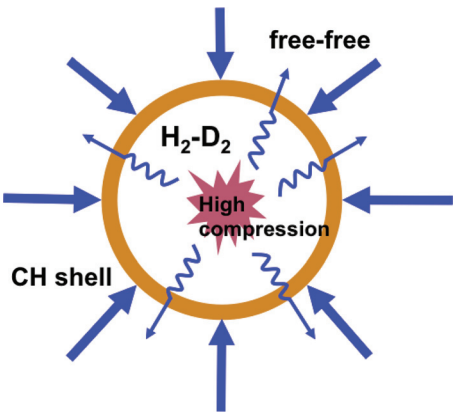

FIG. 4. (Color online) Broadband x-rays can be produced by imploding a spherical CH shell, either unfilled or filled with a low-density gas. A bright burst of bremsstrahlung radiation is produced when the shell stagnates at the center.

II. EXPERIMENTAL SETUP

Experiments were conducted at the Laboratory for Laser Energetics (LLE) in Rochester, NY using either the Omega or Omega EP lasers.[6] Short-pulse target shots were conducted on the Omega EP laser using a single 1 ω (1.053 μm) short-pulse beam with a pulse length of ~74 ps and a focal spot of 200 μm diameter. The maximum on-target energy was ~900 J resulting in an intensity of 4×10^{16} W/cm^2. Long-pulse target shots were also conducted on the Omega EP laser using two 3 ω (0.351 μm) long-pulse beams overlapped in space and time with a pulse length of 1 ns and a focal spot of 150 μm diameter. The total combined energy of the two beams was ~1400 J resulting in an intensity of 8×10^{15} W/cm^2. The imploded CH capsule backlighter measurements were conducted on the Omega laser using a total of 46 beams for a total on-target energy of ~23 kJ in an 1 ns square pulse. Line emission short- and long-pulse targets were 12.5 μm thick, 250 μm disks of either Mo (17 keV) or Ag (22 keV). Broadband emission backlighter targets were spherical plastic capsules of 980 μm diameter with 9 μm thick walls. The capsules were either unfilled or filled with 1 atm Kr gas.

A number of different x-ray diagnostics were employed to cover the x-ray region from 10 keV to 1 MeV. Each diagnostic required careful calibration to extract absolute spectral information from the data. The following sections will describe each diagnostic and its energy range.

A. Single photon counting CCD (5–25 keV)

At the lower end of the x-ray spectrum, single photon counting (SPC) using a CCD camera was employed. A Spectral Instruments SI-800 camera, fitted with a 2048×2048 EEV back-illuminated Si CCD chip, was placed 14 m from the target and collimated using a series of lead apertures placed in series inside an evacuated, light-tight tube. Filters, placed at three locations along the 14 m optical path, were used to reduce the incoming flux incident at the CCD plane to ~1 detected photon per 100 pixels. An incident photon absorbed in the sensitive layer of the CCD transfers its energy to electrons via the photoelectric effect, creating a charge cloud proportional to the energy of the incident x-ray divided by energy required to produce an electron-hole pair in silicon (3.720 eV at liquid nitrogen temperature). The result is an image containing isolated events of intensity proportional to the energy of the incident x-ray photon. A histogram of these events is performed, which results in a trace that resembles the x-ray spectrum. Because the number of detected photons is low, this diagnostic is mostly useful for measuring the conversion efficiency (CE) of laser energy into line emission $T(E)$ photons using the formula,

$$CE = \frac{E \times \text{counts} \times 4\pi}{\epsilon_{\text{eff}}(E) \times T(E) \times \Omega \times E_{\text{laser}}}, \quad (1)$$

where E is the x-ray energy, counts is the number of histogram counts contained in the line emission peak, $\epsilon_{\text{eff}}(E)$ is the counting efficiency of the CCD/histogram combination, Ω is the transmission of the filters, Ω is the solid angle subtended by the CCD, and E_{laser} is the laser energy on-target in the same units as E. The counting efficiency $\epsilon_{\text{eff}}(E)$ is a function of the absorption probability in the Si, the photoelectric fraction, and the probability that the charge cloud will be collected in a single pixel.[7]

B. Crystal spectrometers (10–90 keV)

Two transmission crystal spectrometers were employed, each covering a slightly different x-ray energy range, both designed at the Naval Research Laboratory (NRL). The Double Crystal Spectrometer (DCS) measures from 10 to 80 keV and the Transmission Crystal Spectrometer (TCS) measures from 16 to 90 keV. Both spectrometers use a spherically bent Quartz transmission crystal ($r = 254$ mm) to disperse incoming x-rays, which are then detected on image plates. A schematic diagram of the TCS is shown in the Fig. 5 (inset). The DCS was designed to work with a target-crystal distance of 1 m, whereas the TCS was designed to work at $r = 0.6$ m for better sensitivity. The TCS was absolutely calibrated and used to cross-calibrate the DCS. The calibration of the TCS diagnostic required two separate steps. The first step was to measure the integrated reflectivity of the Quartz crystal. This was performed by Artep Inc. at the National Institute of Standards and Technology (NIST). The integrated reflectivity is shown in Fig. 5(a). The second step was to measure the sensitivity of the image plate detectors to incoming x-rays. Fuji MS (more sensitivity) and SR (super-resolution) image plates were studied and their sensitivity to x-rays was measured at the HEX facility at NSTEC (Ref. 8). Figure 5(b) shows the resulting sensitivity curves. The MS image plates are between 3 and 5 times more sensitive than SR plates and were used as the detectors for the TCS diagnostic to maximize the collected signal. Because thermal recombination in the sensitive region of the image plates causes fading of the data with time, the curve shown in Fig. 5(b) applies only to plates that were scanned 30 min after exposure to x-rays. This fading is also a function of temperature so all plates were kept at room temperature, or 20 °C. The image plates from the TCS diagnostic were scanned 40 min after exposure, corresponding to a 3.5% error in signal due to fading, which is lower than the error bars in the image plate calibration data.

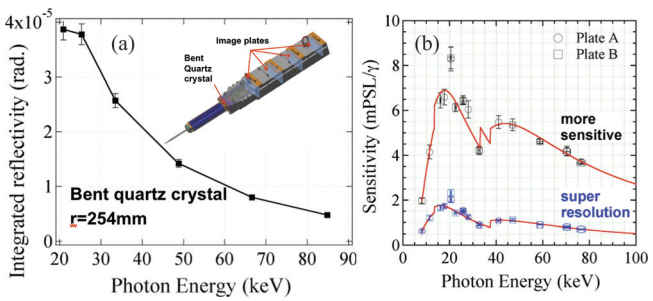

FIG. 5. (Color online) (a) The inset shows a diagram of the TCS spectrometer designed at NRL. The plot shows the integrated reflectivity of the $r = 254$ mm spherically bent transmission quartz crystal measured by Artep Inc. at NIST. (b) Measured sensitivity of MS (more sensitive) and SR (super-resolution) Fuji image plates in units of photo-stimulated luminescence (PSL) per incident photon. Solid lines are fits to the data using a multi-region energy absorption model.

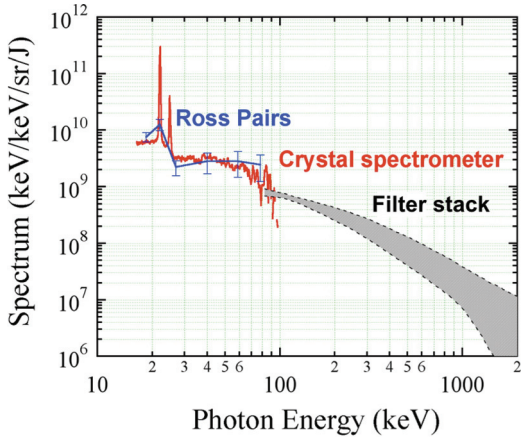

FIG. 6. (Color online) Measured spectrum, in units of KeV of photon energy per keV energy bin per steradian per Joule of laser energy, from a short-pulse driven Ag Kα backlighter using multiple detectors to cover large x-ray range from 16 keV to over 1 MeV.

C. Ross pairs (18–80 keV)

A spectrometer made from differential filters, also known as Ross pairs, was also employed as an additional spectrometer in the 18–80 keV energy range. Ross pairs are convenient because they can provide a very quick, absolute measurement of x-ray spectra, but with coarse energy resolution. A Ross pair is a pair of filters of adjacent or nearly adjacent atomic number with the thicknesses chosen such that the transmission through each filter is the same as outside of their respective K-absorption edges. Thus, the number of photons incident in the energy band bounded by their K-edges is roughly proportional to the difference in signal detected behind the two filters. The Ross pair spectrometer setup used in this study consisted of a 25 μm thick Ta mask with a series of 12 holes of 6 mm diameter cut in a circular pattern in the center. The twelve Ross pair filters are secured over the holes using 12.5 μm thick Kapton tape for a total of six energy bins. The Ta mask/filter assembly is backed by an image plate detector and the entire assembly was housed in a light-tight aluminum clam-shell cartridge during the experiment.

D. Filter stack (80 keV–2 MeV)

For the high-energy bremsstrahlung region, a filter stack spectrometer was used and consists of a series of increasing Z filters, each backed by an image plate detector.[9] The detector response of each image plate detector was calculated as a function of input photon energy using the Integrated Tiger Series (ITS) monte carlo code. Then, the x-ray spectrum emitted from the backlighter target was simulated, also using ITS, for a series of electron distributions and the expected signals on each image plate detector were calculated for each spectra. Finally, least-squares fitting to the experimental data was used to determine the calculated x-ray spectrum that best matched the observed signals.

III. LINE-EMISSION BACKLIGHTERS

Planning and quantitative analysis of radiography experiments and data requires knowledge of the absolute x-ray spectrum of the backlighter source over the entire x-ray energy range spanning the significant detector sensitivity range. To this end, an integrated measurement of the x-ray spectrum of a short-pulse driven Ag backlighter is given in Fig. 6. The TCS crystal spectrometer covers the region from 16 to 80 keV while the filter stack spectrometer covers the x-ray region above 80 keV. A good agreement between the absolute spectrum level and slope is seen between the spectra given by these two instruments. Additionally, Fig. 6 also shows measurements using the Ross pair spectrometer that agree with the TCS data within the experimental error. Thus, Ross pairs can provide a quick, inexpensive, and robust measure of the rough x-ray spectra of these backlighters if energy resolution is not a primary concern.

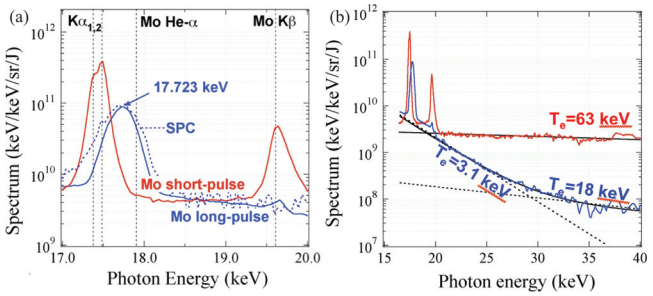

FIG. 7. (Color online) (a) Long- and short-pulse driven Mo spectra in the 17 keV line emission region showing relatively cold $K\alpha_{1,2}$ at 17.479 and 17.374 keV from the short-pulse target and 17.723 line emission from the long-pulse target. The solid red, blue, and dotted lines correspond to short- and long-pulse driven Mo measured using the TCS spectrometer and long-pulse Mo measured by the SPC, respectively. (b) Electron temperature fits to the continuum region of the spectra.

Figure 7(a) shows the line emission region of short- and long-pulse driven Mo backlighters measured using the calibrated TCS spectrometer in the line emission region. The main line emission from the short-pulse driven Mo is consistent with cold $K\alpha_{1,2}$ at 17.479 and 17.374 keV, and the higher energy peak is consistent with $K\beta$ at 17.608 keV. Strong line emission was also observed from the long-pulse driven Mo backlighter with the main peak occurring at 17.72 ± 0.05 keV. This energy is higher than expected for cold Kα, but lower than thermal He-α emission which is expected to be at an x-ray energy of 17.905 keV. Also shown in Fig. 7(a) is a scaled SPC camera histogram showing agreement with a peak energy of 17.72 keV.

To further investigate the long-pulse Mo line emission, the continuum region of the spectrum was fit to derive the effective electron distribution temperatures responsible for the emission. The high energy x-ray continuum spectrum was assumed proportional to $\sim e^{-(E/k_b T_e)}$ (Ref. 10). The resulting T_e was compared to T_{hot} scaling derived by Beg *et al.*, which

TABLE I. Results of fits to the continuum region of short- and long-pulse driven Mo compared to T_{hot} scaling derived by Beg *et al.*

Spectrum	λ (μm)	$I \times 10^{17}$ (W/cm^2)	T_e fit (keV)	T_{hot} fit (keV)
Short-pulse	1.053	0.4	63±7	76
Long-pulse	0.351	0.08	3.1±0.1	—
			18±4	22

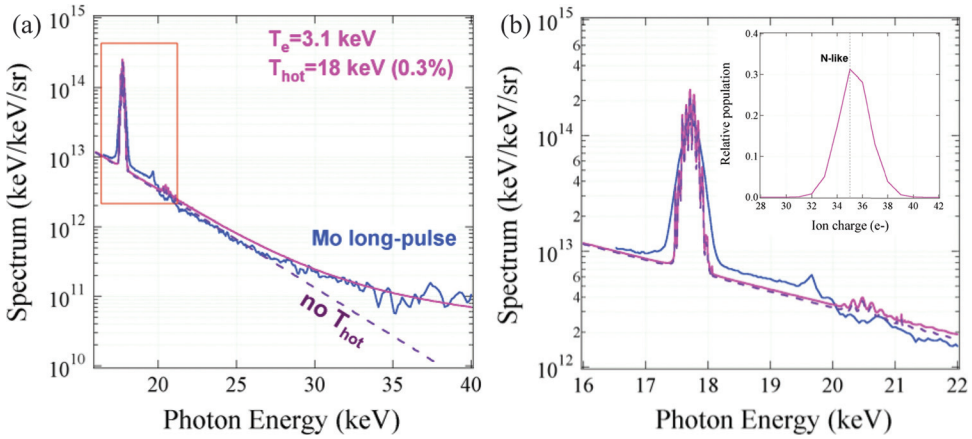

FIG. 8. (Color online) (a) Comparison between the measured Mo long-pulse spectrum and simulations using FLYCHK with (solid) and without (dotted) an 18 keV hot electron distribution. (b) The line emission region is reproduced in both simulations. The inset shows the relative population of ion species from the FLYCHK simulations indicating the dominant ionization state is N-like Mo.

goes as $T_{hot} \sim 100(I\lambda^2)^{1/3}$ with I in units of 10^{17} W/cm^2 and λ in units of microns.[3] The continuum regions and the resulting fits are shown in Fig. 7(b). A comparison of the experimentally inferred electron temperatures with Beg scaling is given in Table I. The inferred electron temperature of 63±7 keV for short-pulse driven Mo agrees reasonably well with the electron temperature predicted by Beg scaling of 76 keV. For long-pulse driven Mo, a two-temperature fit was required to match the shape of the continuum spectrum. The lower-energy thermal component was 3.1±0.1 keV while the higher-energy component of 18±4 keV agrees with Beg scaling within our experimental error.

The long-pulse Mo spectrum was simulated using the atomic physics code FLYCHK with the experimentally inferred electron temperatures as the input along with an electron density of 8×10^{21}, just under the critical density. The results of these simulations compared with the experimental data in the line emission region are shown in Fig. 8(a). The simulations that do not include the 18 keV T_{hot} component do not reproduce the shape of the continuum region above 25 keV whereas the addition of T_{hot} reproduces the data with a hot electron fraction of 0.3%. A closer look at the line emission region is shown in Fig. 8(b). The peak energy and intensity above background is reproduced in both simulations. This implies that the dominant mechanism producing line emission in a long-pulse driven Mo is thermal emission. The inset in Fig. 8(b) shows the relative populations of various Mo ion species from the simulation and indicates that the dominant ionization state is N-like Mo.

The conversion efficiency of laser energy into line emission photons was also measured using single photon counting and compared with previous results. The results are shown in Fig. 3. Although both the short- and long-pulse driven Mo CE are lower than the linear extrapolation from previous data would predict, they both roughly follow previous trends and are within a factor of 3 of each other. Seemingly large variations in the measured conversion efficiency have been seen in many petawatt laser experiments and may be due to a combination of varying laser spot character and target surface finish. At 22 keV (Ag backlighter), the difference between short- and long-pulse backlighter is significantly larger with the long-pulse CE more than an order of magnitude and lower than the short-pulse CE. Combined with the conversion efficiencies at 17 keV, this data suggests the crossover point between long-pulse thermal backlighter CE and short-pulse Kα backlighter CE may be lower than 17 keV, or around 14 keV.

IV. BROADBAND BACKLIGHTERS

The x-ray spectra of broadband imploded CH capsule backlighters were also measured using the DCS crystal spectrometer (cross-calibrated using the TCS calibration) and are shown in Fig. 5(a). A comparison between these spectra and previous measurements from a H_2-D_2 filled capsule measured by Yaakobi *et al.* is given in Fig. 9 (Ref. 11). The absolute spectra measured by Yaakobi *et al.* in the 4.5–7 keV region are higher than the spectra measured here. A simple extrapolation of the slope of the low-energy data, however, intersects the unfilled capsule data near 12 keV. One interesting result that implied by Fig. 9 is that the unfilled capsule x-ray production efficiency is higher than the Kr-filled capsule efficiency above 10 keV. This is in contrast with measurements by Hansen *et al.*, which show the efficiency of a Kr-filled capsule is ~ four times higher than an H_2 filled capsule

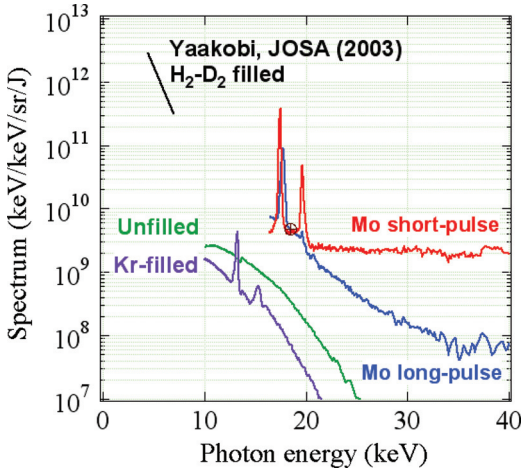

FIG. 9. (Color online) Spectra, in units of KeV of photon energy per keV energy bin per steradian per Joule of laser energy, from unfilled and Kr-filled imploded CH shells compared with previous measurements by Yaakobi *et al.* of a H_2-D_2 filled capsule between 4.5 and 7 keV. Also shown are the long- and short-pulse spectra obtained using the TCS in the same units.

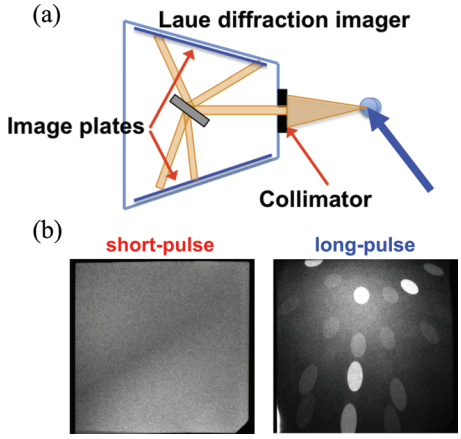

FIG. 10. (Color online) Broadband Laue diffraction using short- and long-pulse driven Mo backlighters. (a) A schematic drawing of the Laue setup consisting of a shielded enclosure made from tungsten alloy and lined with image plate detectors, and a tungsten allow collimator. The crystal is placed inside the enclosure. The backlighter is shown on the right. (b) Laue image using a short-pulse backlighter (left) and a long-pulse backlighter (right). The image on the left is dominated by background.

at 5 keV. This is currently being investigated using hydrodynamics calculations using LASNEX. It is likely that the higher implosion velocity provided by the unfilled capsule, the greater energy per atom for roughly the same *PdV* work, and the higher optical depth of the compressed Kr gas contributes to the greater x-ray emission efficiency of the empty capsule.

Also shown in Fig. 9 are the spectra obtained from long- and short-pulse driven Mo. It is interesting to note that the efficiency of the capsules studied here appears to be much lower than the foil targets in the overlapping measured x-ray regions. The slope of the Mo long-pulse spectra at 16 keV suggests that the efficiency in the 10–16 keV region may also be higher. This suggests that a long-pulse driven Mo foil can be used as an alternative broadband x-ray backlighter in the 10–25 keV region, assuming that the 17 keV line emission and ~1 ns emission time are tolerable. The efficiency of short-pulse driven Mo is also higher. However, background caused by high-energy bremsstrahlung emission from short-pulse petawatt targets can often overwhelm an experiment. This is illustrated in Fig. 10 which shows a broadband Laue experiment using both a short-pulse and a long-pulse driven Mo foil as the backlighter source. Figure 10(a) shows the experimental setup consisting of a shielded tungsten alloy enclosure lined with image plate detectors and a tungsten alloy collimator at the front. The crystal to be studied is placed inside the box and transmission/reflection Laue diffraction is collected on the image plates. As can be seen in Fig. 10(b), no Laue spots are visible in the data taken using the short-pulse backlighter, only a varying background signal. However, many high signal-to-noise Laue spots are visible using a long-pulse Mo backlighter while the background signal is greatly reduced.

V. CONCLUSION

Long- and short-pulse driven Mo and Ag line-emission backlighters were investigated in terms of absolute spectra and conversion efficiency of laser energy into line emission. The effective electron temperatures derived from fits to the continuum region of the Mo spectrum agree well with Beg scaling. Simulations using the atomic physics code FLYCHK indicate that the line emission from long-pulse driven Mo is thermal emission from predominantly N-like Mo ions. Measurements of the conversion efficiency of long- and short-pulse driven backlighters were extended into the crossover region around 17 keV, where it is shown that 17 keV line emission can be obtained with a conversion efficiency roughly 1/3 that of a short-pulse driven backlighter target. These measurements suggest a crossover point of around 14 keV, rather than the predicted 17 keV based on a linear extrapolation of previous measurements of long-pulse conversion efficiency. This result is not too surprising considering the strong dependence of the thermal emission on the laser intensity, a parameter that can vary significantly based on beam quality and other factors, rendering a simple extrapolation from multiple data sets is inaccurate. The absolute spectra from unfilled and Kr-filled imploded CH capsules were also measured. The spectrum from the unfilled capsule is roughly consistent with an extrapolation from low-energy spectral data. It was found that the empty capsule was more efficient at producing 10–25 keV photons than a 1 atm Kr-filled capsule; likely due to the higher implosion velocity provided by the empty capsule, the greater energy per atom for roughly the same PdV work, and the higher optical depth of the compressed Kr gas at peak emission time.

ACKNOWLEDGMENTS

This work was performed under the auspices of the U.S. Department of Energy by Lawrence Livermore National Laboratory under Contract No. DE-AC52-07NA27344.

[1]J. Workman and G. A. Kyrala, Proc. SPIE **4504**, 168 (2001).
[2]L. M. Chen, P. Forget, R. Toth, J. C. Kieffer, A. Krol, C. C. Chamberlain, B. X. Hou, J. Nees, and G. Mourou, Phys. Med. Imaging **5030**, 923 (2003).
[3]F. N. Beg, A. R. Bel, A. E. Dangor, C. N. Danson, A. P. Fews, M. E. Gelinsky, B. A. Hammel, P. Lee, P. A. Norreys, and M. Tatarkis, Phys.Plasmas **4**, 447 (1997).
[4]C. A. Back, J. Grun, C. Decker, L. J. Suter, J. Davis, O. L. Landen, R. Wallace, W. W. Hsing, J. M. Laming, U. Feldman, M. C. Miller, and C. Wuest, Phys. Rev. Lett. **87**, 275003 (2001).
[5]H.-S. Park, B. R. Maddox, E. Giraldez, S. P. Hatchett, L. T. Hudson, N. Izumi, M. H. Key, S. L. Pape, A. J. MacKinnon, A. G. MacPhee, P. K. Patel, T. W. Phillips, B. A. Remington, J. F. Seely, R. Tommasini, R. Town, J. Workman, and E. Brambrink, Phys. Plasmas **15**, 072705 (2008).
[6]T. R. Boehly, R. S. Craxton, T. H. Hinterman, J. H. Kelly, T. J. Kessler, S. A. Kumpman, S. A. Letzring, R. L. McCrory, S. F. B. Morse, W. Seka, S. Skupsky, J. M. Soures, and C. P. Verdon, Rev. Sci. Instrum. **66**, 508 (1995).
[7]B. R. Maddox, H.-S. Park, B. A. Remington, and M. McKernan, Rev. Sci. Instrum. **79**, 10E924 (2008).
[8]B. R. Maddox, H.-S. Park, B. A. Remington, N. Izumi, S. Chen, C. Chen, G. Kimminau, Z. Ali, M. J. Haugh, and Q. Ma, Rev. Sci. Instrum. **82**, 023111 (2011).
[9]C. D. Chen, P. K. Patel, D. S. Hey, A. J. Mackinnon, M. H. Key, K. U. Akli, T. Bartel, F. N. Beg, S. Chawla, H. Chen, R. R. Freeman, D. P. Higginson, A. Link, T. Y. Ma, A. G. MacPhee, R. B. Stephens, L. D. V. Woerkom, B. Westover, and M. Porkolab, Phys. Plasmas **16**, 082705 (2009).
[10]W. Kruer, *Physics of Laser Plasma Interactions* (Addison-Wesley Publishing Co, Reading, MA, 1988).
[11]B. Yaakobi, F. J. Marshall, T. R. Boehly, R. P. J. Town, and D. D. Meyerhofer, J.Opt. Soc. Am. B **20**, 238 (2003).